ACS OMEGA

Open Access

http://pubs.acs.org/journal/acsodf

Article

Apolipoprotein E3 Containing Nanodiscs as Vehicles for Transport and Targeted Delivery of Flavonoid Luteolin

Vernon Gil Laylo Benedicto, Zahraa Haguar, Abbas Abdulhasan, and Vasanthy Narayanaswami*

Cite This: *ACS Omega* 2024, 9, 2988−2999

Read Online

ACCESS | Metrics & More | Article Recommendations | Supporting Information

ABSTRACT: Luteolin is a flavonoid that possesses multiple beneficial biological properties, such as anticancer, antioxidant, and anti-inflammatory effects. The objective of this study is to test the hypothesis that luteolin can be transported across a cell via a nanodisc delivery system and delivered to intracellular sites. Luteolin was incorporated into reconstituted high-density lipoprotein complexes made up of apolipoprotein E3 (apoE3) N-terminal domain (apoE3NT) and 1,2-dimystrioyl-*sn*-*glycero*-3-phosphocholine. ApoE3NT confers the ability on nanodiscs to traverse the plasma membrane via low-density lipoprotein receptor or scavenger receptor-B1. Physicochemical characterization revealed that the nanodiscs were 17−22 nm in diameter as demonstrated by native polyacrylamide gel electrophoresis and dynamic lightering analysis and ∼660 kDa in size, with a luteolin content of ∼4 luteolin molecules/nanodisc. Luteolin appeared to be embedded in the nonpolar core of nanodiscs, as revealed by fluorescence quenching and polarization analysis and spectroscopic characterization. The presence of luteolin did not affect the ability of apoE3NT to mediate binding and cellular uptake of luteolin containing nanodiscs in macrophages, as inferred from immunofluorescence analysis that revealed apoE- and lipid-related fluorescence as punctate perinuclear vesicles and from flow cytometry studies. Lastly, luteolin appeared to be localized in the nucleus, having escaped the lysosomes following disassembly of the nanodiscs as suggested by fluorescence spectroscopy and microscopy analyses. Taken together, nanodiscs offer the potential to effectively transport luteolin and potentially therapeutic drugs into perinuclear sites in cells, where they can be available to enter the nucleus.

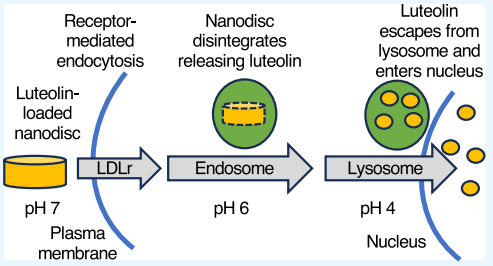

INTRODUCTION

Luteolin (3′,4′,5,7-tetrahydroxyflavone) is a polyphenolic phytochemical (Scheme 1) that has been reported to possess

Scheme 1. Structure of Luteolin

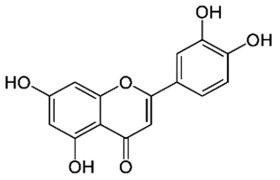

anticancer properties[1−3] similar to several polyphenols through its ability to act as an antioxidant[4] and anti-inflammatory[5−8] agent. In addition, its anticancer activity is also mediated by its ability to mediate cell cycle arrest[9] and to suppress cell survival strategies and stimulating apoptotic strategies (reviewed in[2]). It is also reported as an inhibitor of mast cells that release histamine and cytokines in response to allergens and during immune response.[10] The antioxidant property is conferred by the C3′ hydroxyl group,[11] which plays a critical role as a reducing agent against reactive oxygen species. The anti-inflammatory effect of luteolin stems from its inhibition of COX-2 and inducible nitric oxide synthase, and a decrease in the influx of neutrophils in mice exposed to lipopolysaccharides.[12] As such, it bears substantial potential as a therapeutic agent to delay onset of diseases, including cancer by exerting its pro-apoptotic, antiproliferative, cell cycle arrester, and antioxidant effects.

Nevertheless, its poor solubility in an aqueous medium, such as the blood, has decreased its bioavailability and transportability and limits its use as a therapeutic agent. Luteolin can potentially be encapsulated into liposomes and nanostructured lipid carriers, such as polyethylene glycol.[13] However, they lack targeting ability, can diffuse into cells indiscriminately, and can undergo redistribution with lipoproteins in plasma. In this study, we propose to incorporate luteolin into reconstituted high-density lipoproteins (rHDL), which opens the door for its use as a therapeutic agent. rHDL mimic nascent HDL that are generated during HDL biogenesis, when lipid-free or lipid-poor apolipoprotein (apo) such as apoAI or apoE accept lipids effluxed via ATP binding cassette transporter A1 (ABCA1).[14] The nascent HDL is

Received: November 16, 2023
Revised: December 13, 2023
Accepted: December 15, 2023
Published: January 3, 2024

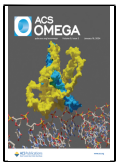

composed predominantly of phospholipids that are arranged as a bilayer surrounded by a belt of apolipoprotein and is discoidal in shape.[15] Lipoproteins resembling nascent HDL can be generated in vitro from commercially available synthetic phospholipids and purified apolipoproteins and offer an excellent mechanism to incorporate and transport nonpolar agents.[16−20]

rHDL are synthetic protein−lipid binary complexes termed nanodiscs that can be reconstituted using apoE3 (or apoAI) and phospholipids (such as phosphatidylcholine and phosphatidylglycerol). The assemblage is a well characterized protocol that yields a high quantity of uniformly sized (10−20 nm) particles.[19] ApoE3 is an exchangeable apolipoprotein that can exist in a lipid-free and lipid-associated state and plays a critical role in cholesterol and triglyceride homeostasis in the plasma and the central nervous system. It is composed of two domains, an N-terminal domain (NT) (residues 1−191) and a C-terminal (CT) domain (residues 201−299)[21] that are linked via a protease-sensitive loop. The NT domain is composed of a four-helix bundle with four long amphipathic α-helices that are arranged in an up-and-down manner[22,23] and folded such that the hydrophobic residues face the protein interior and the hydrophilic residues face toward the aqueous environment. Upon interaction with lipid vesicles, the NT domain undergoes a large conformational change involving opening of the helix bundle and interaction of the hydrophobic face of the helices with the fatty acyl chains of the phospholipids, forming a belt circumscribing the bilayer. In the lipid-associated state, the NT domain has the ability to bind to the low-density lipoprotein receptor (LDLr) family of proteins that promotes receptor-mediated endocytosis and internalizes the entire lipoprotein particle. The isolated NT domain is an independently folded domain, which in the lipid-bound state, retains its ability to bind the LDLr and the scavenger receptor class B type 1B1 (SR-B1).[14] We exploit this feature in the current study and employed a minimalist approach to prepare nanodiscs with the NT domain of apoE3 (apoE3NT) and incorporated luteolin into the hydrophobic interior of nanodiscs. We test the hypothesis that nanodiscs are effective transport vehicles for luteolin and that they deliver the flavonoid to intracellular sites. We report that the incorporation of luteolin into nanodiscs does not compromise the structural integrity of the particle or the ability of apoE3NT to interact with the LDLr and transport luteolin to intracellular sites. The findings offer further proof of concept for the use of nanodiscs for controlled release of biomolecules with similar chemical behavior as luteolin for medical applications.

RESULTS

Preparation of rHDL/Lut. In initial studies, rHDL was prepared in the absence or presence of luteolin with DMPC, DMPG, DMPE, or POPC, and apoE3NT via the cosonication or cholate dialysis method and isolated using density-gradient ultracentrifugation. The continuous gradient that was generated following ultracentrifugation was fractionated and a protein assay was carried out on each fraction to qualitatively locate the presence of protein. Figure 1 shows the absorbance at 562 nm of the different fractions for reconstitution with DMPC in the absence or presence of luteolin. The corresponding profiles for DMPG, DMPE, and POPC are shown in Figure S1. The three fractions with the highest absorbance toward the top of the tube were combined in each case, with the rationale that lipid-associated protein would migrate toward the top of the KBr gradient with the lowest density at the top, while lipid-free or lipid-poor protein would bear higher density and will be located toward the bottom of the tube. Usually, the majority of the top fraction (fraction #1) is composed of protein-free or protein-poor lipid vesicles. In the case of DMPC and POPC fractions 2, 3, and 4 were pooled, while for DMPG it was fractions 3, 4, and 5. In the case of DMPE, we did not observe any trend of migration of lipid-associated proteins in the presence or absence of luteolin in the top fractions.

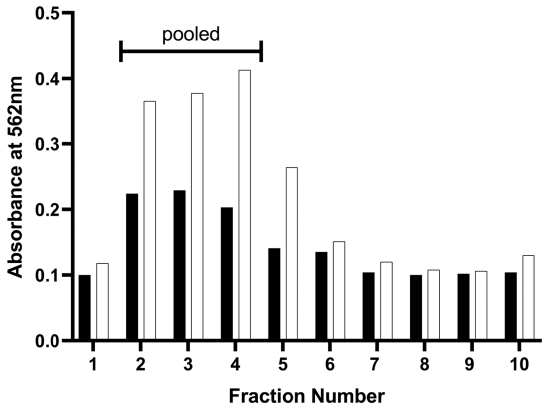

Figure 1. Location of apoE3 NT protein in fractions following ultracentrifugation of rHDL in the absence and presence of luteolin. rHDL was prepared in the absence (white) or presence (black) of luteolin with DMPC and apoE3NT and subjected to density-gradient ultracentrifugation as described under Methods. The continuous gradient that was generated following ultracentrifugation was separated into 10 fractions (#1 being the top and #10 being the bottom fraction) and a BCA protein assay carried out with 10 μL from each fraction. The bar represents fractions with highest absorbance toward the top that were pooled.

In addition, apoAI was tested as an alternate protein component of nanodiscs with DMPC or POPC (Figure S2). Both HDL/apoAI and HDL/apoE3 serve as ligands for SR-B1 aka the "HDL receptor" to deliver core nonpolar components into the cells by a process called selective uptake;[14] however, apoE3 was selected for all studies since it has the additional advantage of facilitating receptor-mediated endocytosis by serving as a ligand for the LDLr family of proteins,[24] which offers more points of cellular entry.

In subsequent experiments, DMPC and apoE3NT were used for all of the reconstitution purposes to generate rHDL with luteolin (rHDL/lut). The pooled fractions were used in subsequent experiments following centrifugal filtration or desalting to remove KBr and unincorporated luteolin.

Physical Characterization of the rHDL/lut Lipoprotein Complex. Particle size and molecular mass of rHDL and rHDL/lut were determined by native polyacrylamide gel electrophoresis (PAGE), as shown in Figure 2 (left). In both cases, large protein/lipid complexes of about 650 kDa mass and ∼15 nm particle diameter were observed. The particle diameter was also independently assessed by dynamic light scattering (DLS) measurements; the plot of size distribution versus intensity (Figure 2, right) indicated that rHDL/lut complexes were significantly larger ($P < 0.0001$) than empty nanodiscs (22.3 ± 0.5 nm and 17.1 ± 0.8 nm ($n = 6$), respectively). Table 1 shows the hydrodynamic properties of rHDL/lut compared with those of rHDL; there was no significant difference in the zeta potential of rHDL (21.5 ± 4.0

https://doi.org/10.1021/acsomega.3c09120
ACS Omega 2024, 9, 2988−2999

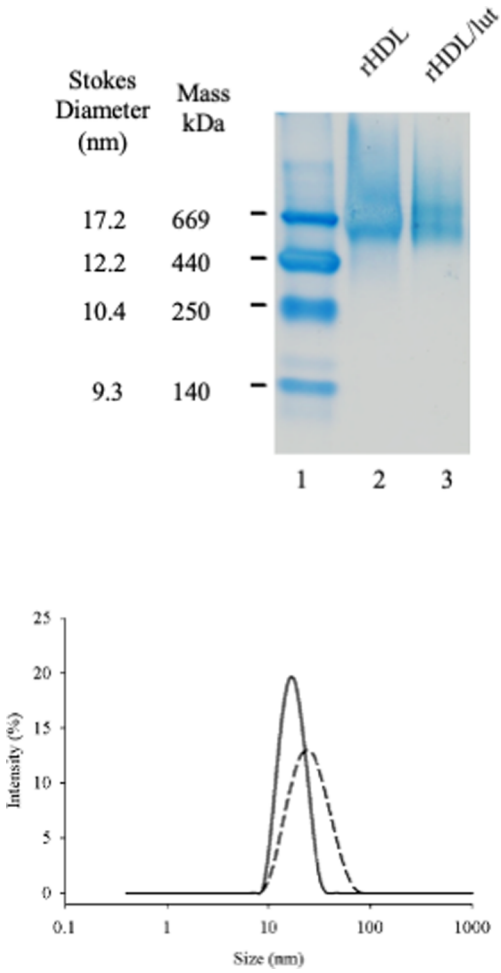

Figure 2. Physical characterization of rHDL/lut. About 10 μg of rHDL and rHDL/lut were loaded onto a 4−20% gradient acrylamide gel, electrophoresed at 60 V for 24 h at 4 °C under nondenaturing conditions and stained overnight with Instant Blue for visualization (left). Lane 1 shows the reference proteins (from top, thyroglobulin, ferritin, catalase, and albumin), with Stokes' diameter and molecular masses indicated on the left. Lane 2, rHDL and Lane 3, rHDL/lut. Particle size was also assessed from the linear-log plot of intensity (%) versus size (nm) by DLS measurements (right) of rHDL (solid) and rHDL/lut (dashed).

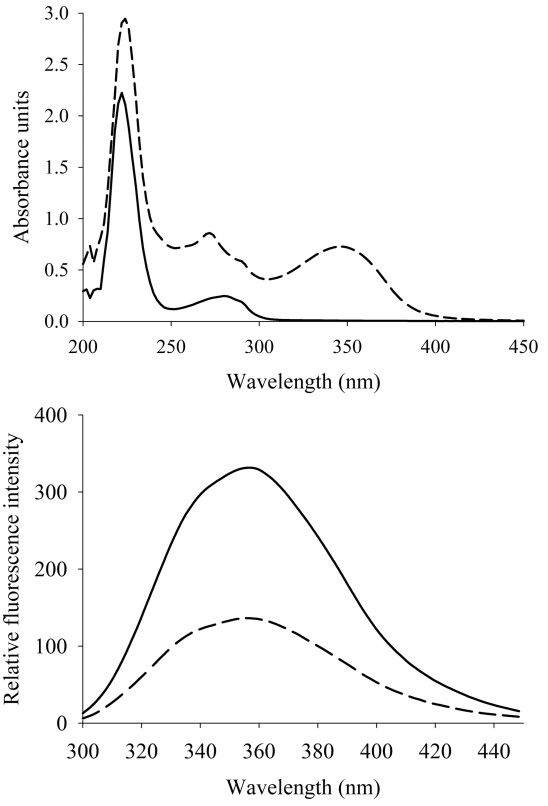

Figure 3. Spectroscopic characterization of rHDL/lut. The UV−vis (top) and the intrinsic fluorescence emission (bottom) spectra of rHDL (solid) and rHDL/lut (dashed) were recorded in PBS. The protein concentrations were ∼1.0 and 0.1 mg/mL, for the absorption and emission spectra, respectively. An average of three scans were recorded per sample. The fluorescence emission spectra were recorded from 295 to 450 nm at an excitation wavelength of 280 nm. The excitation and emission slit widths were set at 3 nm, and the scan speed at 100 nm/min.

mV) and rHDL/lut (20.2 ± 2.8 mV) (n = 6). The PDI for rHDL and rHDL/lut were 0.102 ± 0.037 and 0.169 ± 0.016, respectively (n = 6).

Spectroscopic Characterization of the rHDL/lut Lipoprotein Complex. The absorption spectrum of rHDL/lut (Figure 3, top) reveals a peak at 350 nm that is attributed to luteolin, while that at 280 nm is assigned to the protein, which is also observed from the spectrum of empty nanodiscs. The concentration of luteolin in rHDL/lut was calculated to be 0.127 ± 0.0113 mM (n = 3) from a standard curve of plot of absorbance at 348 nm versus known concentrations of luteolin in dimethyl sulfoxide (DMSO). The larger size of the rHDL/lut particles may be explained by the higher content of phospholipids in these particles as noted from the compositional analysis, which revealed lipid/protein ratios of 67:1 (compared to 39:1 for rHDL), and the presence of ∼4 luteolin molecules/nanodisc (Table 1).

Figure S3 shows the fluorescence emission spectra of luteolin in DMSO and rHDL/lut following excitation at 350

Table 1. Physical Characterization of rHDL/lut and rHDL from native PAGE and DLS Measurements[a]

Measured parameters	rHDL	rHDL/lut	approach	
Stokes diameter (nm)	∼15	∼15	native PAGE	
molecular mass (kDa)	∼650	∼650	native PAGE	
nanodisc diameter (nm)	17.1 ± 0.8*	22.3 ± 0.5*	DLS	n = 6
PDI	0.102 ± 0.037**	0.169 ± 0.016**	DLS	n = 6
zeta potential (mV)	21.5 ± 4.0	20.2 ± 2.8	DLS	n = 6
lipid/protein ratio	39:1	67:1	protein and phospholipid assay	n = 3
number of luteolin/nanodisc		∼4	UV−vis	n = 3

[a]Values expressed are mean ± SD; data analyzed with a two-tailed unpaired t test (*P < 0.0001; **P = 0.005).

https://doi.org/10.1021/acsomega.3c09120
ACS Omega 2024, 9, 2988−2999

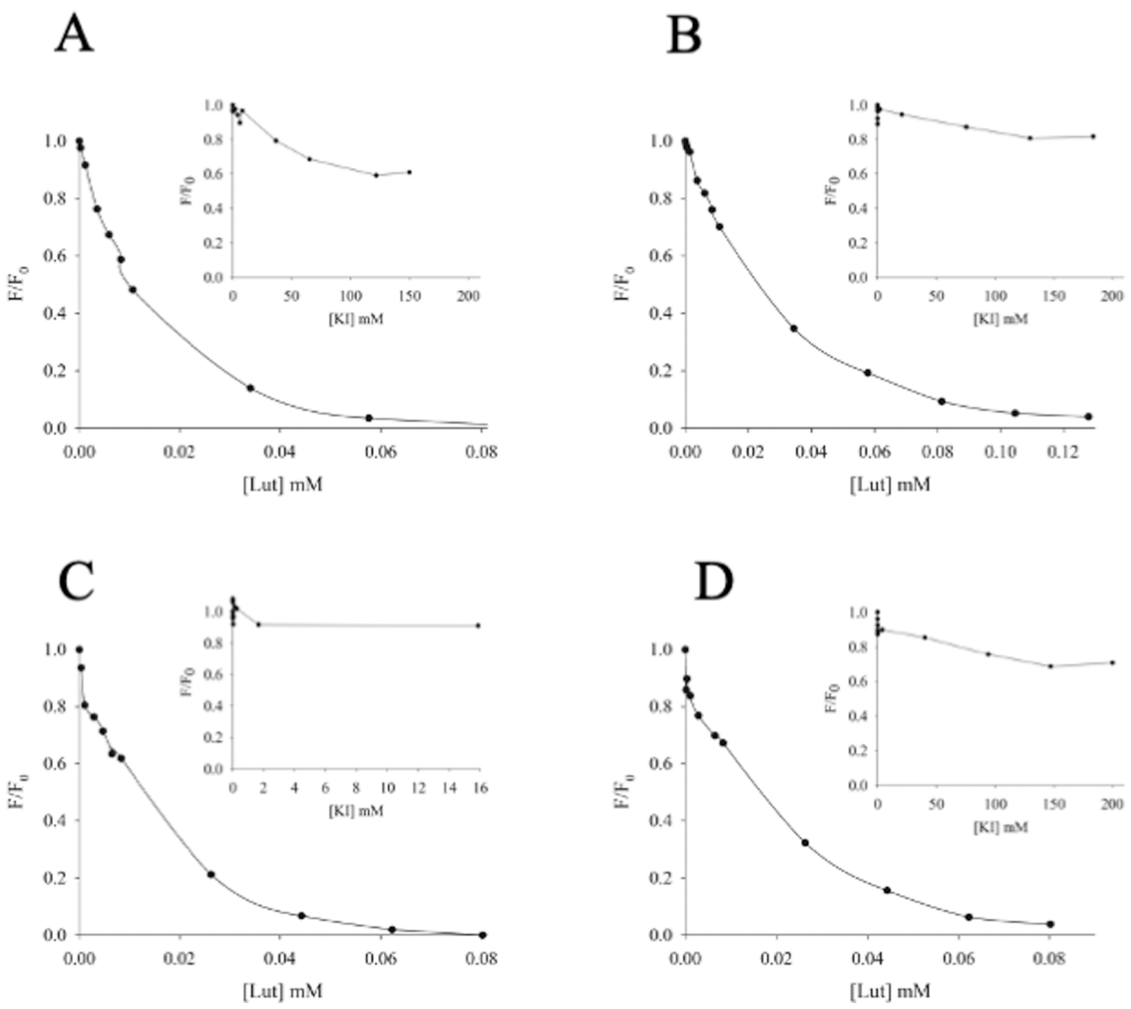

Figure 4. Quenching of intrinsic fluorescence of BSA, LDL, HDL, and rHDL by luteolin and KI. Quenching of intrinsic fluorescence of BSA (A), LDL (B), HDL (C), and rHDL (D) by luteolin was followed by monitoring fluorescence emission intensity at 340 or 356 nm as described under Methods. The excitation wavelength was set at 280 nm and the slit widths at 3 nm. Inset in each panel shows quenching of intrinsic fluorescence by KI.

nm. The two major peaks (428 and 454 nm) in rHDL/lut appear to be blueshifted by about 35 nm compared to the spectrum of luteolin in DMSO, suggesting that luteolin is located in a relatively hydrophobic environment in the nanodiscs.

The intrinsic fluorescence emission spectrum of rHDL/lut (Figure 3, bottom) following excitation at 280 nm revealed significant quenching of Trp emission intensity by ~40% at the the wavelength of maximal fluorescence emission (λ_{max}) of 356 nm compared to that of empty nanodiscs, suggesting incorporation of luteolin in nanodiscs. Luteolin could be associated with the protein circumscribing the periphery facing the aqueous environment at the surface, or in contact with the phospholipid headgroup or buried deep in the nanodisc's nonpolar interior in the large lipoprotein complex.

Determination of Luteolin Incorporation and Location in the Nanodiscs. To further investigate the incorporation and location of luteolin in the nanodiscs, three independent approaches were employed:

1. In the first approach, a comparison of quenching of intrinsic fluorescence emission intensity (F) of Trp/Tyr (referred to as Trp throughout) by increasing amounts of luteolin in different lipoprotein complexes (LDL, HDL, and rHDL) and BSA (a protein with large number of hydrophobic binding sites) was carried out and compared with fluorescence emission intensity in the absence of luteolin (F_0). The rationale is that BSA and all lipoprotein complexes offer nonpolar environments typically occupied by amino acids with hydrophobic side chains, including Trp and Tyr; these residues offer the attractive feature of being intrinsically fluorescent, the changes in which can be monitored. in the A shift in the λ_{max} and/or a decrease in the emission intensity upon addition of luteolin would be an indicator of luteolin's presence in the immediate vicinity of Trp/Tyr residues.

Figure 4 shows plots of F/F_0 versus luteolin concentration for quenching fluorescence of BSA, LDL, HDL, and rHDL (panels A–D, respectively). Luteolin quenches Trp fluorescence emission in a concentration-dependent manner up to 60–100 μM in all four environments that were tested indicative of luteolin's proximity to the Trp/Tyr side chains, which are typically oriented toward a nonpolar environment. DMSO, the vehicle for dissolving luteolin caused negligible or no quenching at the levels used throughout

https://doi.org/10.1021/acsomega.3c09120
ACS Omega 2024, 9, 2988−2999

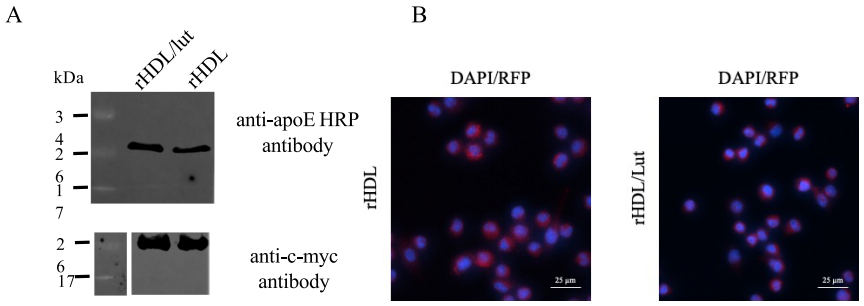

Figure 5. LDLr binding activity and cellular uptake of rHDL/lut. The sLDLr binding ability of rHDL/lut was monitored by the co-IP assay (A) using myc-tagged sLDLr. Empty nanodiscs were used in parallel as control. About 10 μg protein of rHDL or rHDL/lut was incubated with 10 μg of sLDLr at 4 °C for 1 h, followed by co-IP with anti-c-myc agarose. ApoE bound to sLDLr was detected by western blot using HRP-conjugated polyclonal apoE antibody. sLDLr was detected by anti-c-myc antibody for comparison. Cellular uptake of rHDL/lut by J774 cells was monitored by immunofluorescence (B). J774 cells were treated with 10 μg/mL rHDL or rHDL/lut followed by treatment with mAb1D7 (1:1000), Alexa-555 labeled goat antimouse secondary antibody (1:1000) and DAPI. The images were captured using the 375/461 nm channels for DAPI and 540/555 nm RFP channel for Alexa-555.

the study (≤2% v/v). The quenching follows the order HDL > rHDL > BSA > LDL.

2. In the second approach, a comparison of quenching of Trp emission in BSA, LDL, HDL, and rHDL by KI, a polar quencher was carried out to assess accessibility of the fluorophores from the polar side. The rationale is that a comparison of quenching curves between nonpolar and polar quenchers would offer information about the quenchers' environment and location. Plots of F/F_0 for concentration-dependent quenching of BSA, LDL, HDL, and rHDL by KI are shown in Figure 4, Inset, A–D, respectively. Compared to luteolin, KI was a poor quencher of fluorescence in LDL, HDL, and rHDL, at concentrations up to 15–200 mM. In contrast, the intrinsic fluorescence was quenched by ∼40% by KI in BSA, suggesting that the Trp and Tyr in BSA were more accessible to quenching by polar quenchers in BSA, and far less accessible in LDL, HDL, and rHDL.
3. In the third approach, fluorescence polarization (FP) technique was employed to assess incorporation of luteolin into nanodiscs since it measures molecular rotation. Since luteolin has poor fluorescence emission, we employed an extrinsic fluorophore 5-[2-(iodoacetamido)ethylamino]naphthalene-1-sulfonic acid (AEDANS) for FP measurements as described previously.[25] Since the degree of polarization is inversely correlated to its tumbling rate, typically FP values can be used to determine binding of small molecules (which tumble fast) to large proteins or complex assemblies (which tumble slower). In the present case, the single Cys on apoE3NT was labeled with AEDANS prior to reconstitution of the nanodiscs in the absence or the presence of luteolin. rHDL containing AEDANS-apoE3NT and DMPC in the absence or presence of luteolin was prepared as described above. A progressive increase in FP was noted going from lipid-free AEDANS-apoE3NT to rHDL/AEDANS-apoE3NT (0.345–0.378) reflective of binding of lipid-free protein to nanodiscs, and to 0.421 in rHDL/lut/AEDANS-apoE3NT. The slower tumbling of rHDL/lut is attributed to its larger size compared to empty nanodiscs. To validate the use of this approach, the FP value of chemically denatured (6 M guanidine HCl) lipid-free AEDANS-apoE3NT was measured and found to be 0.275. The lower value compared to the folded AEDANS-apoE3NT is indicative of the protein being predominantly unfolded and unstructured by the denaturant. Taken together, the fluorescence data suggest that luteolin is incorporated into the nanodiscs, and likely transitioned to the hydrophobic core of the rHDL particles. The particles were stable under the preparation and storage conditions at pH 7.0 (4 °C for ∼3 months).

LDLr Binding of rHDL/lut and Predicting Release of Luteolin at the Target Site in Lysosomes. Having confirmed luteolin's location in the nonpolar interior of nanodiscs, we next determined if the presence of luteolin affects the LDLr binding ability of apoE3NT using a co-IP assay with c-myc-tagged soluble LDLr (sLDLr) (Figure 5A). The sLDLr (∼26 kDa) bears a portion of the extracellular domain of the LDLr (ligand binding domain LA3–LA6) that is sufficient for binding the ligand (lipoprotein-bound apoE) and is considered a "mini-receptor".[26] The presence of a 24 kDa band corresponding to apoE3NT in the co-immunoprecipitation (co-IP) assay with rHDL/lut indicates that the presence of luteolin did not impair the LDLr binding ability of apoE3NT in the nanodiscs. It is anticipated that upon binding to cellular LDLr, the rHDL/lut would be targeted to and the luteolin released in the lysosomes following receptor-mediated endocytosis. Preliminary solution studies were carried out to obtain support that the embedded luteolin would be released in the environment encountered in lysosomes. rHDL/lut was incubated with Glu-C, an endoprotease that cleaves the CT end of acidic residues at pH 4.0 in the absence or presence of TX-100 to enable solubilization. For comparison, treatment with trypsin was carried out as well at pH 7.0 in the absence or presence of detergent. Sodium dodecyl sulfate-polyacrylamide gel electrophoresis (SDS-PAGE) analysis revealed degradation of apoE3NT scaffold by proteases, Figure S4, panel A. Native PAGE analysis revealed breakdown of rHDL/lut in the presence of proteases or detergent, Figure S4, panel B. Further, to confirm the release of luteolin upon particle disintegration, Trp fluorescence emission spectra of rHDL/lut was recorded at pH 4 after treatment with buffer or detergent for 24 h, Figure S4, panel C. Compared to rHDL, the fluorescence emission of Trp remained quenched at pH 7.0 after 24 h in rHDL/lut, as shown previously in Figure 3. At pH 4.0, a further decrease in fluorescence emission of rHDL/lut

https://doi.org/10.1021/acsomega.3c09120
ACS Omega 2024, 9, 2988–2999

was noted with a shift in λ_{max} by ∼8 nm from 360 to 352 nm in the absence of detergent. In the presence of detergent, a significant recovery of fluorescence after release of quenching by luteolin was noted to levels seen with empty nanodiscs. It was necessary to use a detergent such as SDS since it causes particle disaggregation but allows us to monitor Trp fluorescence emission of the intact protein. SDS was the detergent of choice since it is well-known that TX-100 shows significant interference in fluorescence emission noted for Trp. Taken together, these data reveal particle disintegration and the release of luteolin under conditions encountered in lysosomes.

Cellular Uptake of rHDL/lut. Subsequently, cellular uptake of rHDL/lut was monitored in J774 macrophages, a cell line selected since they do not synthesize any endogenous apoE. The cells were treated with rHDL or rHDL/lut (10 μg/mL) and visualized by immunofluorescence using anti-apoE antibody mAb1D7 and Alexa-555 labeled goat antimouse antibody (Figure 5B). In both cases, cellular fluorescence was noted as punctate, perinuclear vesicles, indicating that the presence luteolin did not affect the uptake of rHDL/lut by receptor-mediated endocytosis.

Subsequently, flow cytometry was used to obtain a quantitative measure of uptake of DiI/rHDL or DiI/rHDL/lut in cells, as shown in Figure 6. Both exhibited a similar median fluorescence intensity (MFI) confirming that the presence of luteolin did not affect the cellular uptake of nanodiscs. The samples containing luteolin, DMSO, rHDL, and rHDL/lut (that were used as negative controls) did not exhibit a fluorescence emission due to the absence of DiI. Figure S5 shows the gated population of cells as dot plots for cells exposed to DiI/rHDl and DiI/rHDL/lut, revealing that exposure to the nanodiscs did not affect the viability of the cells or cause cell death.

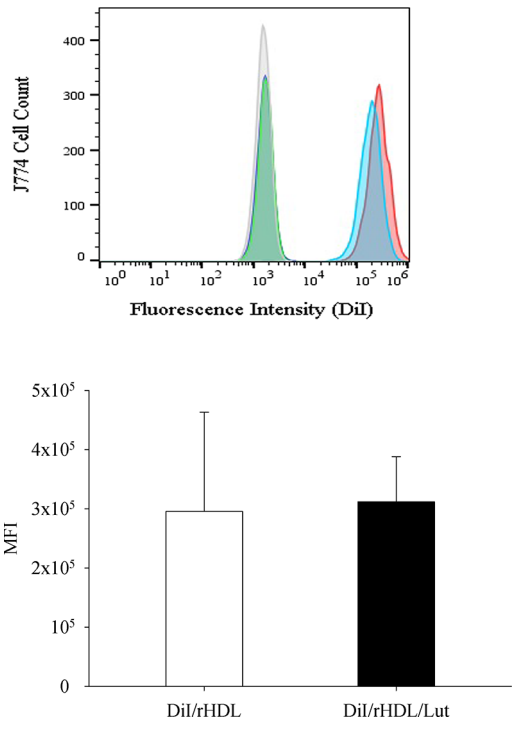

Figure 6. Histograms of cell associated fluorescence intensity for J774 cells exposed to DiI/rHDL and DiI/rHDL/lut. J774 cells were exposed to PBS (purple), luteolin (green), rHDL/lut (gray), DiI/rHDL (blue), or DiI/rHDL/lut (red). About 6000 cells were analyzed and the MFI at 575 nm used for analysis. Representative histograms are shown from three biological replicate experiments using cells of various passages (top). The MFI for cells exposed to DiI/rHDL and DiI/rHDL/lut (bottom) are represented quantitatively (bottom).

Cellular Uptake of rHDL/lut Visualized Using DPBA, Enhancer of Luteolin Fluorescence. Although flavonoids tend to display fluorescence emission properties, they are weak for use as such in cellular studies, which precludes their use for direct fluorescence visualization in cells. One way to circumvent this problem is by using DPBA, a chemical used to enhance fluorescence emission in flavonoids.[27] Other researchers showed that treatment of the flavonoid 5,3′,4′-tridmethylnobiletin with 2-aminoethyl diphenylborinate (DPBA) resulted in enhanced fluorescence that allowed visualization in Caco-2 cells.[28] To determine if this is applicable to luteolin as well, an initial analysis of the luteolin−DPBA mixture was carried out in solution studies to verify if luteolin's fluorescence emission is enhanced by DPBA. Luteolin and DPBA were mixed in 1:1 molar ratio (20 μM each) to form a conjugate as described by previous studies.[28] The fluorescence emission of the luteolin/DPBA mixture was monitored following excitation at 490 nm and compared with that of free DPBA (Figure 7, top). The λ_{max} values of free DPBA and free luteolin were found to be 532 and 524 nm, respectively. The luteolin/DPBA mixture exhibited a λ_{max} at 560 nm, registering a redshift of 28 and 36 nm, respectively, indicative of formation of a conjugate. Furthermore, the mixture exhibited a 15× increase in fluorescence intensity compared to DPBA alone and ∼2× increase compared to luteolin alone. The enhanced fluorescence of the conjugate prompted us to apply this approach to directly visualize cellular uptake of luteolin in macrophages in the presence of DPBA by fluorescence microscopy.

Cellular uptake of rHDL/lut was carried out as described above and compared to those treated with lut (Figure 7, bottom); the cells were stained with DPBA in the last step after DAPI staining prior to image capture. A more intense green fluorescence was noted in the nuclei for cells treated with rHDL/lut in the presence of DPBA compared with those treated with lut.

DISCUSSION

The naturally occurring flavonoid, luteolin, offers a wide range of benefits with its anticancer,[9,29,30] antiproliferative, and apoptotic properties. In addition, it also mediates anti-inflammatory effects by inhibiting the production of inflammatory markers (such as VEGF, IL-6 and IL-8, TNF-α, IL-1β)[8,31,32] and antioxidant activity by its radical scavenging properties;[33−35] further, it offers protection against carbon tetrachloride-induced hepatic toxicity[33] and cisplatin-induced kidney toxicity.[36] As such, these attributes prompt researchers to investigate its therapeutic potential and to deliver it in an appropriate vehicle to a desired target site. Given its lipophilicity, luteolin has been delivered to cells or administered intraperitoneally dissolved in solvents such as DMSO. In an effort to identify delivery systems for therapeutic purposes, newer systems are being developed involving nanoparticles. In this study, we characterized nanodiscs with incorporated luteolin and reported the potential use of this system to deliver it to intracellular sites. There are many advantages of delivering flavonoids in nanodiscs versus solvents. It is envisaged that when administered dissolved in

https://doi.org/10.1021/acsomega.3c09120
ACS Omega 2024, 9, 2988−2999

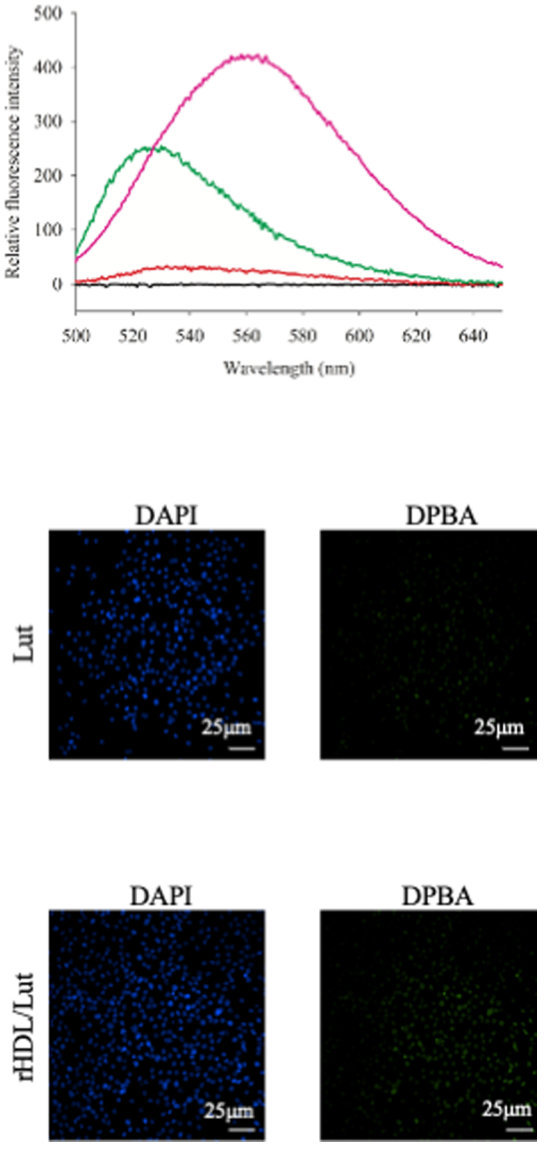

Figure 7. Cellular uptake of rHDL/lut visualized using DPBA, an enhancer of luteolin fluorescence. Fluorescence emission spectra (top) of DMSO (black), 20 μM DPBA (red), 20 μM luteolin (green) and 20 μM luteolin +20 μM DPBA (pink) were recorded following excitation at 490 nm. The spectra were recorded with 3 nm excitation and emission slit widths at a scan speed of 100 nm/min. Direct fluorescence imaging of J774 cells treated with luteolin or rHDL/lut (bottom), stained with DAPI and DPBA. Images were captured using the GFP (480/560 nm) and DAPI (375/461 nm) channels.

solvents, the flavonoids will transition to the different lipoproteins in the blood or bind albumin, as shown by the fluorescence studies in the current study. They tend to get "diluted" in the plasma, thereby necessitating administration at higher concentrations. On the other hand, when they are packaged in nanodiscs, they are limited to the lipoprotein environment and are more bioavailable. Further, they can be administered as a water-soluble preparation, thereby eliminating the need for solvent. The diameter (15−20 nm) and geometry (discoidal) of nanodiscs are ideal for drug transport.[37] Lastly, the flexible nature of apoE3NT and modular and self-assembling nature of nanodiscs make them more attractive for drug transport compared to administration in the solvent.[19] This study takes advantage of these properties and provides proof of concept for the use of nanodiscs with apoE3NT for transporting other nutraceuticals or drugs of similar size, solubility, and chemical nature, with potential to extend its application to therapeutic targeting.

Previous studies have demonstrated that phospholipids with saturated 14 carbon chain fatty acyl groups (myristoyl) and phosphocholine headgroup were the optimal lipid components of nanodiscs with different apolipoproteins (apoAI, apoE3, apoLp-III, apoE3NT, apoECT domain),[15−17,38−42] yielding stable binary complexes. For the current study with luteolin, we employed the NT domain of apoE3 as the protein component because of its ability (i) to facilitate receptor-mediated endocytosis via the LDLr family of proteins and (ii) to form larger nanodiscs with ∼15 nm diameter and ∼650 kDa mass as reported by others investigating nanolipoproteins formulations.[41] The larger size could potentially accommodate more cargo. For determining the phospholipid component, we carried out an initial screen of 14:0 phospholipids with three different headgroups (DMPC, DMPG, and DMPE) in addition to a major phospholipid in naturally occurring HDL (POPC) as possible lipid components for nanodiscs with luteolin (Figure S1). Of the phospholipids tested (Table S1, Supporting Information), DMPC, DMPG, and POPC were viable options for luteolin incorporation (based on ability to form isolatable lipoprotein complexes during density-gradient ultracentrifugation that could be detected by nondenaturing PAGE (data not shown for DMPG and POPC). Several studies have focused on characterizing protein-containing nanodiscs prepared from various phospholipids differing in charge.[43−45] In particular, the presence of anionic phospholipids such as DMPG appears to decrease aggregation due to charge−charge repulsion between nanodiscs and confer stability to the nanodiscs due to the interaction of the headgroup with the protein belt.[45] The nature of the cargo also determines the choice of phospholipids; for example, binary mixtures containing DMPC and cationic lipids, such as dimyristoyltrimethylaminopropane or polycations, such as polyamines may be used for transporting nucleic acids.[46,47] In the current study, DMPC and apoE3NT were selected as the lipid and protein of choice for incorporating luteolin since DMPC/apoE3NT nanodiscs are well characterized and offer a stable environment for incorporating hydrophobic molecules, such as luteolin. Based on molecular composition (protein and luteolin concentrations) and mass and particle diameter (native PAGE and DLS) analyses, it was estimated that reconstitution with DMPC, apoE3NT, and luteolin yielded ∼4 luteolin molecules per nanodisc.

The nanodisc presents three locations for the accommodation of small molecules: the amino acid side chains of apoE3NT facing the aqueous exterior, the phosphocholine headgroup of DMPC, and the interior of the lipoprotein complexin the fatty acyl core of the phospholipids, including the protein/lipid interface wherein the nonpolar side chains of the amphipathic helices of apoE3NT face the fatty acyl chain. The sites on the protein belt facing the aqueous environment were less likely to accommodate and bind luteolin, given the predominantly hydrophobic nature of the molecule. Quenching analysis of Trp fluorescence emission is a classical method used for determining the binding or location of small molecules in proteins or lipoproteins. It has been used to demonstrate the binding of a variety of plant-derived polyphenolic antioxidants to serum albumin and LDL.[48] It is well established that albumin has a remarkable ability to bind a

https://doi.org/10.1021/acsomega.3c09120
ACS Omega 2024, 9, 2988−2999

large range of chemically diverse nonpolar molecules, which is a critical factor in drug and nutraceutical transport, pharmacokinetics, and efficacy.[49,50] In the current study, quenching of Trp emission in BSA was used as an indicator of luteolin binding to the hydrophobic pockets on the protein, though the precise binding location is not known. In a similar manner, fluorescence quenching analysis was used to identify the location of luteolin in the hydrophobic interior of LDL and HDL, roughly spherical particles composed of a monolayer of amphipathic lipids and proteins and a core of neutral lipids. Trp residues on proteins, such as apoB100 on LDL and apoAI on HDL (major proteins on these particles), typically face the particle interior. Quenching of the Trp fluorescence by luteolin suggests that luteolin is located in the nonpolar core of the lipoprotein particle. A similar inference was made of Trp quenching by luteolin in rHDL, though in this case, luteolin is likely to be intercalated between the fatty acyl chains of the nanodisc's phospholipid bilayer. Trp quenching occurred both under conditions where luteolin was included during the reconstitution step and when it was added in incremental amounts to empty nanodiscs. Conversely, iodide, an aqueous quencher, caused negligible quenching of Trp fluorescence in the empty nanodiscs and in HDL and LDL. A similar observation was made in studies involving the location of curcumin (diferuloylmethane), a polyphenolic flavonoid, in nanodiscs;[16] in this case, the fluorescence emission of curcumin was quenched efficiently by DOXYL-fatty acids, which partition directly into the lipid bilayer, but not by iodide. FP measurements suggested the presence of luteolin in nanodiscs. Additional support for luteolin localization was derived from the blueshifted λ_{max} of luteolin fluorescence emission, which informs about the nonpolar environment of the fluorophore.

Taken together, these biophysical data confirm that luteolin is embedded in the hydrophobic interior of the nanodisc. While native PAGE analysis suggested differences in nanodisc diameter and mass, DLS measurements indicated a significantly increased diameter in rHDL/lut. The presence of the apolipoproteins acts as a "belt" to hold a bilayer of phospholipids in the nanodiscs with the embedded cargo, offering potential to improve their half-life in the blood. It is estimated that ∼4 apoE3NT may be present per discoidal particle from compositional analysis. It may be possible to increase the load of luteolin, a concept triggered by recent findings from computational simulations of nanodiscs with four apoE3NT molecules with varying amounts of DMPC.[51] The simulation predicted the formation of stable binary complexes with 240−420 DMPC molecules/nanodisc. Experimental data from the current study revealed ∼160 and ∼280 phospholipids per nanodisc for rHDL and rHDL/lut, respectively. The increase in diameter and size of rHDL/lut may be attributed to the presence of luteolin, which may disrupt the close packing of the fatty acyl chains of the nanodisc bilayer, allow recruitment of more apoE3NT and, consequentially, promote recruitment of more phospholipids. The rHDL/lut particles were stable under the preparation and storage conditions (4 °C for ∼3 months at pH 7.0) and, as expected, were susceptible to degradation in environments such as those found in the lysosomes. Importantly, the presence of luteolin did not impair the functional ability of the apoE3NT domain to interact with the LDLr as deduced from co-IP with sLDLr. The retention of the functional ability of the apoE3NT domain was further noted in fluorescence microscopy images of macrophages treated with rHDL/lut. Flow cytometry data indicated that the cellular uptake of rHDL/lut was quantitatively similar to that of rHDL.

Lastly, luteolin appeared to be localized in the nuclei following cellular internalization. As expected, the rHDL/lut particles likely disintegrated in the low pH environment of the lysosomes (pH 4−5), thereby releasing embedded luteolin. This was shown in solution studies, where the environment encountered in lysosomes was simulated by exposing rHDL/lut to proteases acting at pH 4, which degraded apoE3NT that scaffolded the nanodisc and released the embedded luteolin. Given that luteolin bears multiple sites that can be deprotonated, it is reasonable to propose that it would exist in a neutral protonated form (although the precise pK_a values of luteolin are not known) in the low pH milieu of the lysosome, which may allow lysosomal escape by diffusion through the membrane and partitioning into the nuclei. It is noteworthy that luteolin localizes in the nucleus, where it can target the DNA in the cancer cells and mediate its antiproliferative effect by inducing apoptosis[52] or by G0/G1, S, or G2/M phase cell cycle arrest[9,52,53] or decreasing cell proliferation[9] or suppressing matrix metalloproteinase that support cancer metastasis[54] (and reviewed in refs 1 and 2). Interestingly, similar nuclear localization was reported when curcumin, a polyphenol was delivered to glioblastoma cells via apoE-containing discoidal particles.[55] Overall, given that there is sufficient evidence for the beneficial role of luteolin as an anticancer, antioxidant, and anti-inflammatory agent, its mode of delivery can be refined with nanodiscs offering a potentially improved mode of delivery to target sites such as the nucleus for biomedical applications.

METHODS

Luteolin (99+% pure) was obtained from TSZ CHEM (Fisher Scientific), and 1-palmitoyl-2-oleoyl-*sn-glycero*-3-phosphocholine (POPC), 1,2-dimystrioyl-*sn-glycero*-3-phosphocholine (DMPC), 1,2-dimyristroyl-*sn-glycero*-3-phosphoglycerol (DMPG), 1,2-dimyristroyl-*sn-glycero*-3-phosphoethanolamine (DMPE), were purchased from Avanti Polar Lipids, Inc. (Alabaster, AL). The phospholipid assay kit was purchased from WAKO Chemicals USA, Inc. (Richmond, VA). The DC and BCA protein assay kits were from Bio-Rad Laboratories (Hercules, CA) and ThermoScientific (Rockford, IL), respectively. 1,10-Dioctadecyl-3,3,30,30-tetramethyl indocarbocyanine iodide (DiI) was from Invitrogen (Waltham, MA), BSA and LDL were from Sigma-Aldrich (St. Louis, MO) and HDL was from Academy Bio-Medical Company, Inc. (Houston, TX). Mass spectrometry grade trypsin and Glu-C were purchased from Promega (Madison, WI). All solvents used were of analytical grade. 2-Aminoethyl diphenylborinate (DPBA) was a kind gift from Dr. Joe Vinson (University of Scranton, PA).

UV−Vis Spectroscopy of Luteolin and rHDL/lut. In initial studies, the solubility of luteolin at concentrations required for cellular assays was assessed using DMSO, DMF, methanol, and ethanol. The absorbance spectra of increasing concentrations of luteolin (0.01−0.10 mg/mL) dissolved in DMSO were recorded from 200 to 600 nm. The average of triplicate measurements was used to determine the concentration of luteolin in rHDL (described below) by generating a standard curve of absorbance at 348 nm versus a known concentration of luteolin.

https://doi.org/10.1021/acsomega.3c09120
ACS Omega 2024, 9, 2988−2999

Fluorescence Spectroscopy. All fluorescence spectra were recorded at a scan speed of 100 nm/min (typically an average of 5 scans) in a PerkinElmer LS-55B Luminescence Spectrometer with excitation and emission slit widths set between 3 and 10 nm. Trp/Tyr fluorescence emission was recorded from 300 to 500 nm following excitation at 280 nm. Luteolin fluorescence was followed from 360 to 600 nm upon excitation at 350 nm. Luteolin-DPBA conjugate emission was monitored from 500 to 700 nm following excitation at 490 nm. Luteolin-DPBA conjugates were prepared by mixing 20 mM DPBA in water with 20 mM luteolin in DMSO at a 1:1 ratio in a glass test tube. The emissions of luteolin and DPBA alone were monitored to note their individual contribution.

Fluorescence Analysis. The binding of luteolin to BSA, HDL, LDL, and rHDL was examined indirectly as quenching of intrinsic fluorescence due to Trp/Tyr in the proteins. Fluorescence emission spectra of BSA (~250 μg), HDL (~150 μg), LDL (~500 μg), and rHDL (~100 μg) were recorded in the absence of luteolin following excitation at 280 nm. Increasing concentrations of stock solutions of luteolin in DMSO (0.2, 2.0, and 20 mM) or KI (0.2, 2.0, 20, 40, 400 mM, 4 M, and 6 M) were added to the different protein solutions in 20 mM sodium phosphate buffer, pH 7.4 containing 150 mM NaCl (phosphate buffered saline, PBS) and the fluorescence intensity at 340 nm (for HDL) or 356 nm (for BSA, LDL, and rHDL) recorded. The KI stock solutions contained 1 mM sodium thiosulfate to prevent the formation of free iodine. In experiments where luteolin was added, the final concentration of DMSO was maintained to be <2% v/v. In control reactions, the effect of adding increasing volumes of DMSO (data not shown) was recorded at the respective emission wavelength to account for possible fluorescence emission quenching by vehicle alone. The absorbance of luteolin at 280 nm was $\ll$0.1 at the concentrations used thereby contributing minimally to any inner filter effect. ApoE3NT labeled with 5-[2-(Iodoacetamido)ethylamino]naphthalene-1-sulfonic acid (AEDANS) was used for FP measurements as described previously.[25] The excitation and emission wavelengths were set at 340 and 480 nm, respectively, with 5 nm slit width and integration time of 15 s for a total period of about 3 min.

Dynamic Light Scattering. DLS measurements were performed using a Zetasizer 3000 HSA (HORIBA Ltd., Sunnyvale, CA) to measure particle diameter, polydispersity index (PDI), and zeta potential of rHDL/lut preparations. The samples were present at apoE3NT concentrations of 1−2 mg/mL in PBS at 25 °C. Typically, three technical replicates of three biological replicates of rHDL and rHDL/lut were studied for collecting data.

Reconstitution and Characterization of rHDL with Luteolin. Recombinant human apoE3 residues 1−191 bearing a hexa-His tag at the N-terminal end was overexpressed in *Escherichia coli,* isolated and purified using a Ni-affinity matrix (Hi-Trap chelating column, G.E. Healthcare, Uppsala, Sweden) as described earlier.[38] rHDL (also referred to as nanodiscs) containing DMPC or DMPE or DMPG and apoE3NT (5:2 w/w starting ratio) were prepared by the cosonication method as described previously.[16] Nanodiscs containing luteolin were preparedby including 5.0 mg of luteolin while making the lipid film. Lipid-free protein and protein-free lipid were separated from rHDL complexes by density-gradient ultracentrifugation using a KBr gradient. Fractions containing both protein and phospholipid were pooled based on the protein and lipid assay. The concentration of luteolin incorporated into rHDL was quantified based on a standard curve generated as described above. Native PAGE analysis of rHDL with and without luteolin was carried out to estimate the Stokes diameter and molecular mass of the complexes using 4−20% gradient acrylamide gel, electrophoresing at 60 V for 24 h at 4 °C, and staining overnight with Instant Blue. Nanodiscs containing rHDL with incorporated luteolin are referred to as rHDL/lut throughout.

Protease and Detergent Treatment of rHDL/lut. About 10 μg of rHDL/lut was incubated at 37 °C for 24 h with various treatments: (i) PBS, (ii) 0.1% TX-100, (iii and iv) trypsin (1:60 enzyme:protein m/m) in 50 mM sodium phosphate pH 7.0 in the absence or presence of 0.1% TX-100, (v and vi) Glu-C (1:40 enzyme:protein mass ratio) in 50 mM sodium acetate pH 4, Glu-C (1:40 enzyme:protein m/m) in 50 mM sodium acetate pH 4 in the absence or presence of 0.1% TX-100. The samples were subject to SDS-PAGE under reducing conditions or native PAGE. For Trp fluorescence analysis, rHDL/lut (50 μg) was incubated in 50 mM sodium acetate buffer, pH 4.0 at 37 °C for 24 h in the absence or presence of 0.1% SDS. In control reactions, Trp fluorescence emission spectra of rHDL (empty nanodiscs) or rHDL/lut in 50 mM sodium phosphate buffer, pH 7.0 was recorded as described above.

Coimmunoprecipitation. To determine if rHDL/lut retains its ability to bind the LDLr binding, a coimmunoprecipitation (co-IP) assay was performed with a soluble form of the receptor bearing essential ligand binding domains LA3-LA6 as described previously.[26,56] Briefly, 10 μg of soluble LDLr (sLDLr) with a c-myc epitope was incubated with 10 μg of protein samples in their lipid-associated state as rHDL or rHDL/lut in the presence of 2 mM $CaCl_2$ in PBS for 1 h at 4 °C. Anti-c-myc antibody-linked agarose (MilliporeSigma, St. Louis, MO) was used to capture sLDLr/rHDL or sLDLr/rHDL/lut complexes. The presence of apoE3NT was confirmed using a HRP-conjugated polyclonal apoE antibody (1:5000 dilution) (Meridian Life Science, Inc., Memphis, TN), while the presence of sLDLr was confirmed using an anti c-myc antibody (9E10) (1:1000 dilution) (Abcam, Cambridge, UK), and goat antimouse HRP antibody (1:5000 dilution).

Visualization of Cellular Uptake of rHDL/Lut. *By Immunofluorescence.* The uptake of rHDL in cells was visualized by immunofluorescence using an antibody to apoE3NT, mAb1D7 (Lipoproteins & Atherosclerosis Research Group, University of Ottawa Heart Institute, Ottawa, Canada).[57] J774 mouse macrophages were grown to 80% confluency (DMEM, 10% fetal bovine serum, 1× penicillin−streptomycin−glutamine) and split into a μ-Slide 4- or 8-well chambered coverslip (50,000 cells per well) from Ibidi (Gräfelfing, Germany). Following incubation in lipoprotein deficient serum (LPDS) for 24 h to induce overexpression of the LDLr, the cells were washed 3× with DPBS and incubated for 2 h at 37 °C with 10 μg/mL of rHDL or rHDL/lut. The cells were fixed with 3.7% formaldehyde in DPBS for 10 min at 24 °C and permeabilized with 0.2% Triton X-100 for 5 min at 24 °C. Cells were treated with mAb1D7 (1:1000) for 1 h at 37 °C, followed by Alexa-555 labeled secondary antibody (goat antimouse, 1:1000) for 1 h at 37 °C. Cell nuclei were stained with 4′,6-diamidino-2-phenylindole dihydrochloride [DAPI, Research Organics (Cleveland, OH)]. The chambered coverslip was mounted on a glass slide with mounting medium (KPL, Gaithersburg, MD) and stored long-term at −20 °C by sealing the edges of the coverslip. Nikon Eclipse Ti2 E

https://doi.org/10.1021/acsomega.3c09120
ACS Omega 2024, 9, 2988−2999

fluorescence microscope (with a 60× objective) was used to visualize the cells. In all studies, empty nanodiscs with no added luteolin were used at similar concentrations as the control.

By Direct Visualization. In other studies, the lipid component of the rHDL/lut complex was monitored using DiI, a lipid-based fluorescent probe that was incorporated into rHDL/lut. It facilitates direct visualization by fluorescence microscopy, in addition to quantification by flow cytometry as described previously.[57,58] Briefly, about 50 μL of a stock solution of DiI (0.3 mg/mL) in DMSO (Alfa Aesar, HPLC grade, 99.9% Ward Hill, MA, USA) was incubated with rHDL or rHDL/lut in PBS for 18 h at 37 °C in the dark. Unbound DiI was separated by density-gradient ultracentrifugation as described above, and the sample was filtered through 0.22 μm filter (Waters Millex HV units, SLHV R04 NL Millipore, Carrigtwohill, Co. Cork, Ireland) prior to application to cells. The complexes generated will be termed DiI/rHDL/lut or DiI/rHDL, and their cellular uptake monitored as described above and visualized directly at 565 nm.

Using DPBA Enhancer of Luteolin Fluorescence. The uptake of luteolin was visualized using DPBA as an enhancer of luteolin fluorescence as reported by Chen et al.[28] J774 macrophages were grown to 80% confluency, split into a μ-Slide 4- or 8-well chambered coverslip (ibidi GmbH, Gräfelfing, Germany) (50,000 cells per well) and allowed to adhere overnight. They were incubated in a LPDS medium for 24 h, followed by treatment with 10 μg/mL of rHDL or rHDL/lut mixed in the LPDS medium (500 μL/well) for 2 h at 37 °C. In parallel, cells were treated with 20 μM luteolin or DMSO (<5 μL) mixed in the LPDS medium. The cells were then washed three times with DPBS, fixed, permeabilized, and stained with DAPI, as described above. The cells were then stained with 20 μM DPBA in water for 30 min at 37 °C and slides were prepared for visualization as described above. Cells were visualized using the GFP (480/560 nm) and DAPI (375/461 nm) channels. Images captured at 40× magnification.

Quantitative Assessment of rHDL/lut Uptake by Flow Cytometry. The uptake of rHDL/lut in cells was quantified by flow cytometry using a Sony Cell Sorter SH800. J774 macrophages (~300,000/well) were grown in 6-well culture plates to 100% confluency and pretreated with LPDS. The cells were then treated with DiI/rHDL/lut or DiI/rHDL as described above, detached with CellStripper (Corning, NY), centrifuged at 600 rpm for 5 min at 4 °C, resuspended, and washed 3× with fluorescence-activated cell sorting (FACS) buffer (Hanks Balanced Salt Solution + 1% BSA + 0.05% sodium azide) at 4 °C. They were then resuspended in 250 μL of FACS buffer, examined using the 488 nm laser with the phycoerythrin (PE) filter, and analyzed by flow cytometry FlowJo software (v10.8.1, Tree Star, Ashland, OR). The MFI values were plotted for each treatment. Cells treated with PBS, 20 μM luteolin, and rHDL were used as controls.

Statistical Analysis. For all analyses, data are represented as mean ± SD based on three independent experiments. Calculations for two-tailed unpaired Student's t test were performed by GraphPad (GraphPad software, La Jolla, CA) and Microsoft Excel. P values <0.05 were considered statistically significant.

■ ASSOCIATED CONTENT

Supporting Information

The Supporting Information is available free of charge at https://pubs.acs.org/doi/10.1021/acsomega.3c09120.

Location of apoE3 NT protein in fractions following ultracentrifugation of rHDL in the absence and presence of luteolin; location of apoAI protein in fractions following ultracentrifugation of rHDL in the absence and presence of luteolin; fluorescence emission spectra of luteolin in DMSO and rHDL/lut in PBS; effect of disrupting particle integrity of rHDL/lut; plot of forward scatter versus side scatter of J774 macrophages exposed to DiI/rHDL or DiI/rHDL/lut; and summary of apolipoproteins and phospholipids tested for luteolin incorporation (PDF)

■ AUTHOR INFORMATION

Corresponding Author

Vasanthy Narayanaswami − *Department of Chemistry and Biochemistry, California State University, Long Beach, Long Beach, California 90840, United States;* orcid.org/0000-0001-7088-4057; Phone: 1-562 985 4953; Email: vas.narayanaswami@csulb.edu; Fax: 1-562 985 8557

Authors

Vernon Gil Laylo Benedicto − *Department of Chemistry and Biochemistry, California State University, Long Beach, Long Beach, California 90840, United States;* Present Address: Capsida Biotherapeutics, 1300 Rancho Conejo Boulevard, Thousand Oaks, California 91320, United States; orcid.org/0000-0002-0257-8303

Zahraa Haguar − *Department of Chemistry and Biochemistry, California State University, Long Beach, Long Beach, California 90840, United States*

Abbas Abdulhasan − *Department of Chemistry and Biochemistry, California State University, Long Beach, Long Beach, California 90840, United States*

Complete contact information is available at: https://pubs.acs.org/10.1021/acsomega.3c09120

Author Contributions

V.G.L.B.: conceptualization; data acquisition; formal analysis; investigation; methodology; writing-original draft, review and editing; Z.H.: data acquisition; formal analysis; investigation; methodology; A.A.: data acquisition; formal analysis; investigation; methodology; V.N.: conceptualization; formal analysis funding acquisition; investigation; methodology; project administration; supervision; writing-original draft, review and editing. All authors approve the final version of the manuscript.

Notes

The authors declare no competing financial interest.

■ ACKNOWLEDGMENTS

This work was supported by the National Institutes of Health (grant # NIH-GM105561 (V.N.), NIH R25GM071638 (V.B.)), NSF LSAMP Program fellowship (HRD-182649 (A.A. and Z.H.)) and CSULB MD Alumni Program (Z.H.). The funding sources were not involved in the study design, data collection, data analysis, or interpretation. We thank Brendan Ly and Kyla Anderson for their initial help and Drs.

Arti Patel and Theoharis Theoharides for initiating our interest in the project and for continued intellectual input.

■ ABBREVIATIONS

DMPC: 1,2-dimystrioyl-*sn-glycero*-3-phosphocholine; LDLr: low-density lipoprotein receptor; rHDL: reconstituted high-density lipoprotein

■ REFERENCES

(1) Imran, M.; Rauf, A.; Abu-Izneid, T.; Nadeem, M.; Shariati, M. A.; Khan, I. A.; Imran, A.; Orhan, I. E.; Rizwan, M.; Atif, M.; Gondal, T. A.; Mubarak, M. S. Luteolin, a Flavonoid, as an Anticancer Agent: A Review. *Biomedicine & Pharmacotherapy* **2019**, *112*, No. 108612.

(2) Seelinger, G.; Merfort, I.; Wölfle, U.; Schempp, C. Anti-Carcinogenic Effects of the Flavonoid Luteolin. *Molecules* **2008**, *13* (10), 2628−2651.

(3) Lin, Y.; Shi, R.; Wang, X.; Shen, H.-M. Luteolin, a Flavonoid with Potential for Cancer Prevention and Therapy. *CCDT* **2008**, *8* (7), 634−646.

(4) Seelinger, G.; Merfort, I.; Schempp, C. Anti-Oxidant, Anti-Inflammatory and Anti-Allergic Activities of Luteolin. *Planta Med.* **2008**, *74* (14), 1667−1677.

(5) Chen, C.-Y.; Peng, W.-H.; Tsai, K.-D.; Hsu, S.-L. Luteolin Suppresses Inflammation-Associated Gene Expression by Blocking NF-κB and AP-1 Activation Pathway in Mouse Alveolar Macrophages. *Life Sciences* **2007**, *81* (23−24), 1602−1614.

(6) Hwang, J.-T.; Park, O. J.; Lee, Y. K.; Sung, M. J.; Hur, H. J.; Kim, M. S.; Ha, J. H.; Kwon, D. Anti-Tumor Effect of Luteolin Is Accompanied by AMP-Activated Protein Kinase and Nuclear Factor-κB Modulation in HepG2 Hepatocarcinoma Cells. *Int. J. Mol. Med.* **2011**, *28*, 25−31, DOI: 10.3892/ijmm.2011.667.

(7) Song, Y. S.; Park, C. M. Luteolin and Luteolin-7-O-Glucoside Strengthen Antioxidative Potential through the Modulation of Nrf2/MAPK Mediated HO-1 Signaling Cascade in RAW 264.7 Cells. *Food Chem. Toxicol.* **2014**, *65*, 70−75.

(8) Weng, Z.; Patel, A. B.; Vasiadi, M.; Therianou, A.; Theoharides, T. C. Luteolin Inhibits Human Keratinocyte Activation and Decreases NF-κB Induction That Is Increased in Psoriatic Skin. *PLoS One* **2014**, *9* (2), No. e90739.

(9) Knowles, L. M.; Zigrossi, D. A.; Tauber, R. A.; Hightower, C.; Milner, J. A. Flavonoids Suppress Androgen-Independent Human Prostate Tumor Proliferation. *Nutrition and Cancer* **2000**, *38* (1), 116−122.

(10) Weng, Z.; Patel, A. B.; Panagiotidou, S.; Theoharides, T. C. The Novel Flavone Tetramethoxyluteolin Is a Potent Inhibitor of Human Mast Cells. *J.Allergy Clini.Immunol.* **2015**, *135* (4), 1044−1052.

(11) Noroozi, M.; Angerson, W. J.; Lean, M. E. Effects of Flavonoids and Vitamin C on Oxidative DNA Damage to Human Lymphocytes. *American Journal of Clinical Nutrition* **1998**, *67* (6), 1210−1218.

(12) Zeng, P.; Zhang, Y.; Pan, C.; Jia, Q.; Guo, F.; Li, Y.; Zhu, W.; Chen, K. Advances in Studying of the Pharmacological Activities and Structure−Activity Relationships of Natural C-Glycosylflavonoids. *Acta Pharmaceutica Sinica B* **2013**, *3* (3), 154−162.

(13) Huang, M.; Su, E.; Zheng, F.; Tan, C. Encapsulation of Flavonoids in Liposomal Delivery Systems: The Case of Quercetin, Kaempferol and Luteolin. *Food Funct.* **2017**, *8* (9), 3198−3208.

(14) Phillips, M. C. Molecular Mechanisms of Cellular Cholesterol Efflux. *J. Biol. Chem.* **2014**, *289* (35), 24020−24029.

(15) Raussens, V.; Fisher, C. A.; Goormaghtigh, E.; Ryan, R. O.; Ruysschaert, J. M. The Low Density Lipoprotein Receptor Active Conformation of Apolipoprotein E. Helix Organization in n-Terminal Domain-Phospholipid Disc Particles. *J. Biol. Chem.* **1998**, *273* (40), 25825−25830.

(16) Khumsupan, P.; Ramirez, R.; Khumsupan, D.; Narayanaswami, V. Apolipoprotein E LDL Receptor-Binding Domain-Containing High-Density Lipoprotein: A Nanovehicle to Transport Curcumin, an Antioxidant and Anti-Amyloid Bioflavonoid. *Biochim. Biophys. Acta* **2011**, *1808* (1), 352−359.

(17) Kim, S. H.; Adhikari, B. B.; Cruz, S.; Schramm, M. P.; Vinson, J. A.; Narayanaswami, V. Targeted Intracellular Delivery of Resveratrol to Glioblastoma Cells Using Apolipoprotein E-Containing Reconstituted HDL as a Nanovehicle. *PLoS One* **2015**, *10* (8), No. e0135130.

(18) Chuang, S. T.; Shon, Y.-S.; Narayanaswami, V. Apolipoprotein E3-Mediated Cellular Uptake of Reconstituted High-Density Lipoprotein Bearing Core 3, 10, or 17 Nm Hydrophobic Gold Nanoparticles. *Int. J. Nanomedicine* **2017**, *12*, 8495−8510.

(19) Chuang, S. T.; Cruz, S.; Narayanaswami, V. Reconfiguring Nature's Cholesterol Accepting Lipoproteins as Nanoparticle Platforms for Transport and Delivery of Therapeutic and Imaging Agents. *Nanomaterials* **2020**, *10* (5), 906.

(20) Singh, A. T. K.; Ghosh, M.; Forte, T. M.; Ryan, R. O.; Gordon, L. I. Curcumin Nanodisk-Induced Apoptosis in Mantle Cell Lymphoma. *Leukemia & Lymphoma* **2011**, *52* (8), 1537−1543.

(21) Weisgraber, K. H. Apolipoprotein E: Structure-Function Relationships. *Adv. Protein Chem.* **1994**, *45*, 249−302.

(22) Wilson, C.; Wardell, M. R.; Weisgraber, K. H.; Mahley, R. W.; Agard, D. A. Three-Dimensional Structure of the LDL Receptor-Binding Domain of Human Apolipoprotein E. *Science* **1991**, *252* (5014), 1817−1822.

(23) Chen, J.; Li, Q.; Wang, J. Topology of Human Apolipoprotein E3 Uniquely Regulates Its Diverse Biological Functions. *Proc. Natl. Acad. Sci. U.S.A.* **2011**, *108* (36), 14813−14818.

(24) Phillips, M. C. Apolipoprotein E Isoforms and Lipoprotein Metabolism. *IUBMB Life* **2014**, *66* (9), 616−623.

(25) Yang, L.; Hernandez, R. V.; Tran, T. N.; Nirudodhi, S.; Beck, W. H. J.; Maier, C. S.; Narayanaswami, V. Ordered Opening of LDL Receptor Binding Domain of Human Apolipoprotein E3 Revealed by Hydrogen/Deuterium Exchange Mass Spectrometry and Fluorescence Spectroscopy. *Biochimica et Biophysica Acta (BBA) - Proteins and Proteomics* **2018**, *1866* (11), 1165−1173.

(26) Fisher, C.; Abdul-Aziz, D.; Blacklow, S. C. A Two-Module Region of the Low-Density Lipoprotein Receptor Sufficient for Formation of Complexes with Apolipoprotein E Ligands. *Biochemistry* **2004**, *43* (4), 1037−1044.

(27) Córdoba, A.; Satué, M.; Gómez-Florit, M.; Hierro-Oliva, M.; Petzold, C.; Lyngstadaas, S. P.; González-Martín, M. L.; Monjo, M.; Ramis, J. M. Flavonoid-Modified Surfaces: Multifunctional Bioactive Biomaterials with Osteopromotive, Anti-Inflammatory, and Anti-Fibrotic Potential. *Adv. Healthcare Mater.* **2015**, *4* (4), 540−549.

(28) Chen, J.; Song, M.; Wu, X.; Zheng, J.; He, L.; McClements, D. J.; Decker, E.; Xiao, H. Direct Fluorescent Detection of a Polymethoxyflavone in Cell Culture and Mouse Tissue. *J. Agric. Food Chem.* **2015**, *63* (49), 10620−10627.

(29) Fotsis, T.; Pepper, M. S.; Aktas, E.; Breit, S.; Rasku, S.; Adlercreutz, H.; Wähälä, K.; Montesano, R.; Schweigerer, L. Flavonoids, Dietary-Derived Inhibitors of Cell Proliferation and in Vitro Angiogenesis. *Cancer Res.* **1997**, *57* (14), 2916−2921.

(30) Ko, W. G.; Kang, T. H.; Lee, S. J.; Kim, Y. C.; Lee, B. H. Effects of Luteolin on the Inhibition of Proliferation and Induction of Apoptosis in Human Myeloid Leukaemia Cells. *Phytother. Res.* **2002**, *16* (3), 295−298.

(31) Wang, S.; Cao, M.; Xu, S.; Zhang, J.; Wang, Z.; Mao, X.; Yao, X.; Liu, C. Effect of Luteolin on Inflammatory Responses in RAW264.7 Macrophages Activated with LPS and IFN-γ. *J.Funct.Foods* **2017**, *32*, 123−130.

(32) Kumazawa, Y.; Kawaguchi, K.; Takimoto, H. Immunomodulating Effects of Flavonoids on Acute and Chronic Inflammatory Responses Caused by Tumor Necrosis Factor &#945. *CPD* **2006**, *12* (32), 4271−4279.

(33) Domitrović, R.; Jakovac, H.; Milin, Č.; Radošević-Stašić, B. Dose- and Time-Dependent Effects of Luteolin on Carbon Tetrachloride-Induced Hepatotoxicity in Mice. *Exp.Toxicol.Pathol.* **2009**, *61* (6), 581−589.

https://doi.org/10.1021/acsomega.3c09120
ACS Omega 2024, 9, 2988−2999

(34) Lima, C. F.; Fernandes-Ferreira, M.; Pereira-Wilson, C. Phenolic Compounds Protect HepG2 Cells from Oxidative Damage: Relevance of Glutathione Levels. *Life Sciences* **2006**, *79* (21), 2056−2068.
(35) Oh, H.; Kim, D.-H.; Cho, J.-H.; Kim, Y.-C. Hepatoprotective and Free Radical Scavenging Activities of Phenolic Petrosins and Flavonoids Isolated from Equisetum Arvense. *J.Ethnopharmacol.* **2004**, *95* (2−3), 421−424.
(36) Domitrović, R.; Cvijanović, O.; Pugel, E. P.; Zagorac, G. B.; Mahmutefendić, H.; Škoda, M. Luteolin Ameliorates Cisplatin-Induced Nephrotoxicity in Mice through Inhibition of Platinum Accumulation, Inflammation and Apoptosis in the Kidney. *Toxicology* **2013**, *310*, 115−123.
(37) Florensa, M.; Llenas, M.; Medina-Gutiérrez, E.; Sandoval, S.; Tobías-Rossell, G. Key Parameters for the Rational Design, Synthesis, and Functionalization of Biocompatible Mesoporous Silica Nanoparticles. *Pharmaceutics* **2022**, *14* (12), 2703.
(38) Choy, N.; Raussens, V.; Narayanaswami, V. Inter-Molecular Coiled-Coil Formation in Human Apolipoprotein E C-Terminal Domain. *J. Mol. Biol.* **2003**, *334* (3), 527−539.
(39) Wientzek, M.; Kay, C. M.; Oikawa, K.; Ryan, R. O. Binding of Insect Apolipophorin III to Dimyristoylphosphatidylcholine Vesicles. Evidence for a Conformational Change. *J. Biol. Chem.* **1994**, *269* (6), 4605−4612.
(40) Raussens, V.; Drury, J.; Forte, T. M.; Choy, N.; Goormaghtigh, E.; Ruysschaert, J.-M.; Narayanaswami, V. Orientation and Mode of Lipid-Binding Interaction of Human Apolipoprotein E C-Terminal Domain. *Biochem. J.* **2005**, *387* (Pt 3), 747−754.
(41) Chromy, B. A.; Arroyo, E.; Blanchette, C. D.; Bench, G.; Benner, H.; Cappuccio, J. A.; Coleman, M. A.; Henderson, P. T.; Hinz, A. K.; Kuhn, E. A.; Pesavento, J. B.; Segelke, B. W.; Sulchek, T. A.; Tarasow, T.; Walsworth, V. L.; Hoeprich, P. D. Different Apolipoproteins Impact Nanolipoprotein Particle Formation. *J. Am. Chem. Soc.* **2007**, *129* (46), 14348−14354.
(42) Nath, A.; Atkins, W. M.; Sligar, S. G. Applications of Phospholipid Bilayer Nanodiscs in the Study of Membranes and Membrane Proteins. *Biochemistry* **2007**, *46* (8), 2059−2069.
(43) Bayburt, T. H.; Sligar, S. G. Membrane Protein Assembly into Nanodiscs. *FEBS Lett.* **2010**, *584* (9), 1721−1727.
(44) Bayburt, T. H.; Grinkova, Y. V.; Sligar, S. G. Self-Assembly of Discoidal Phospholipid Bilayer Nanoparticles with Membrane Scaffold Proteins. *Nano Lett.* **2002**, *2* (8), 853−856.
(45) Wadsäter, M.; Maric, S.; Simonsen, J. B.; Mortensen, K.; Cardenas, M. The Effect of Using Binary Mixtures of Zwitterionic and Charged Lipids on Nanodisc Formation and Stability. *Soft Matter* **2013**, *9* (7), 2329.
(46) Ghosh, M.; Ren, G.; Simonsen, J. B.; Ryan, R. O. Cationic Lipid Nanodisks as an siRNA Delivery Vehicle. *Biochem. Cell Biol.* **2014**, *92* (3), 200−205.
(47) Rui, M.; Tang, H.; Li, Y.; Wei, X.; Xu, Y. Recombinant High Density Lipoprotein Nanoparticles for Target-Specific Delivery of siRNA. *Pharm. Res.* **2013**, *30* (5), 1203−1214.
(48) Poloni, D. M.; Dangles, O.; Vinson, J. A. Binding of Plant Polyphenols to Serum Albumin and LDL: Healthy Implications for Heart Disease. *J. Agric. Food Chem.* **2019**, *67* (33), 9139−9147.
(49) Petitpas, I.; Bhattacharya, A. A.; Twine, S.; East, M.; Curry, S. Crystal Structure Analysis of Warfarin Binding to Human Serum Albumin: Anatomy of Drug Site I. *J. Biol. Chem.* **2001**, *276* (25), 22804−22809.
(50) Fasano, M.; Curry, S.; Terreno, E.; Galliano, M.; Fanali, G.; Narciso, P.; Notari, S.; Ascenzi, P. The Extraordinary Ligand Binding Properties of Human Serum Albumin. *IUBMB Life* **2005**, *57* (12), 787−796.
(51) Allen, P.; Smith, A. C.; Benedicto, V.; Abdulhasan, A.; Narayanaswami, V.; Tapavicza, E. Molecular Dynamics Simulation of Apolipoprotein E3 Lipid Nanodiscs. *Biochimica et Biophysica Acta (BBA) -. Biomembranes* **2024**, *1866* (1), 184230.
(52) Chang, J.; Hsu, Y.; Kuo, P.; Kuo, Y.; Chiang, L.; Lin, C. Increase of Bax/ Bcl-XL Ratio and Arrest of Cell Cycle by Luteolin in Immortalized Human Hepatoma Cell Line. *Life Sciences* **2005**, *76* (16), 1883−1893.
(53) Su Bog, Y.; Jung Hwa, L.; Hae Young, C.; Kwang Sik, I.; Song Ja, B.; Jae Soo, C.; Nam Deuk, K. Inhibitory Effects of Luteolin Isolated Fromixeris Sonchifolia Hance on the Proliferation of Hepg2 Human Hepatocellular Carcinoma Cells. *Arch Pharm. Res.* **2003**, *26* (2), 151−156.
(54) Huang, Y.-T.; Hwang, J.-J.; Lee, P.-P.; Ke, F.-C.; Huang, J.-H.; Huang, C.-J.; Kandaswami, C.; Middleton, E.; Lee, M.-T. Effects of Luteolin and Quercetin, Inhibitors of Tyrosine Kinase, on Cell Growth and Metastasis-Associated Properties in A431 Cells Over-expressing Epidermal Growth Factor Receptor: Effects of Tyrosine Kinase Inhibitors on Cell Growth. *Br. J. Pharmacol.* **1999**, *128* (5), 999−1010.
(55) Ghosh, M.; Ryan, R. O. ApoE Enhances Nanodisk-Mediated Curcumin Delivery to Glioblastoma Multiforme Cells. *Nanomedicine* **2014**, *9* (6), 763−771.
(56) Tran, T. N.; Kim, S. H.; Gallo, C.; Amaya, M.; Kyees, J.; Narayanaswami, V. Biochemical and Biophysical Characterization of Recombinant Rat Apolipoprotein E: Similarities to Human Apolipoprotein E3. *Arch. Biochem. Biophys.* **2013**, *529* (1), 18−25.
(57) Cruz, S.; Narayanaswami, V. Cellular Uptake and Clearance of Oxidatively-Modified Apolipoprotein E3 by Cerebral Cortex Endothelial Cells. *IJMS* **2019**, *20* (18), 4582.
(58) Abeer, M. I.; Abdulhasan, A.; Haguar, Z.; Narayanaswami, V. Isoform-specific Modification of Apolipoprotein E by 4-hydroxynonenal: Protective Role of Apolipoprotein E3 against Oxidative Species. *FEBS J.* **2023**, *290*, 3006−3025.

https://doi.org/10.1021/acsomega.3c09120
ACS Omega 2024, 9, 2988−2999